



NRL/FR/6910--12-10,232

Combining Nondeterministic Separation and Chemical Interactions for Concentration of Nanoparticles

ANTHONY P. MALANOSKI

BRANDY J. WHITE

JEFFREY S. ERICKSON

Center for Bio/Molecular Science and Engineering

December 17, 2012

Approved for public release; distribution is unlimited.

This page
intentionally
left blank

CONTENTS

INTRODUCTION	1
APPROACH	2
Reagents	2
Fluorescence	2
Asymmetric Ratchet Devices	3
Surface Functionalization	5
Experimental Setup.....	5
EXPERIMENTS	6
Generation 1 Glass Devices.....	6
Generation 2 Silicon Devices	7
Surface Functionalization	8
Surface Charge.....	8
Other Considerations	13
CONCLUSIONS.....	16
ACKNOWLEDGMENTS	17
REFERENCES	17

FIGURES

Fig. 1	Brownian ratchets.....	1
Fig. 2	Precursors used for wafer functionalization.....	2
Fig. 3	Calibration curve for fluorescent nanospheres.....	3
Fig. 4	Masks used for generation 1 glass devices.....	4
Fig. 5	SEM images before and after mask stripping for generation 1 glass devices.....	4
Fig. 6	Device assembly.....	5
Fig. 7	Nanoparticle concentrations in generation 1 devices.....	6
Fig. 8	Nanoparticle concentrations in functionalized generation 1 devices.....	7
Fig. 9	Nanoparticle solutions of varied pH in generation 1 devices.....	7
Fig. 10	Nanoparticles in water on generation 2 devices.....	9
Fig. 11	Nanoparticle solutions at pH 6.5 on generation 2 devices.....	10
Fig. 12	Nanoparticle solutions at pH 7.5 on generation 2 devices.....	11
Fig. 13	Nanoparticle solutions at pH 9.5 on generation 2 devices.....	12
Fig. 14	Nanoparticle solutions at higher concentration in water.....	14
Fig. 15	Nanoparticle solutions at higher concentration, pH 6.5.....	15
Fig. 16	Nanoparticle solutions at higher concentration, pH 7.5.....	15
Fig. 17	Nanoparticle solutions at higher concentration, pH 9.5.....	16

COMBINING NONDETERMINISTIC SEPARATION AND CHEMICAL INTERACTIONS FOR CONCENTRATION OF NANOPARTICLES

INTRODUCTION

The Center for Bio/Molecular Science and Engineering at the Naval Research Laboratory (NRL) initiated a program in October 2009 to determine the potential utility of separation techniques based on Brownian motion. This type of separation would rely on nondeterministic approaches (biased diffusion). Though this idea had been described and theories were available for gaseous targets and examples based on movement through lipid membranes [1–15], very little work was published on the application of the mechanism for separation of components of liquid solutions. In addition, the NRL study would evaluate the impact of combining chemical functionalities with biased diffusion in an attempt to further enhance the process. The program included device design and development as well as experimental evaluation of the separation efficiencies. Devices were based on the idea of Brownian ratchets: a field of asymmetric shapes used to facilitate differential diffusion (Fig. 1). Smaller particles, for example, have a higher diffusion coefficient, making them more likely to move across a ratchet. The asymmetric shape of the ratchet forces particles that do not make it far enough across to diffuse back to the leading side. The overall result is that smaller particles move further across the field of ratchets, whereas larger particles, diffusing more slowly, are more likely to travel straight through the device. With a large enough field of ratchets and a large enough difference in the rates of diffusion of particles, a noticeable separation should be observed.

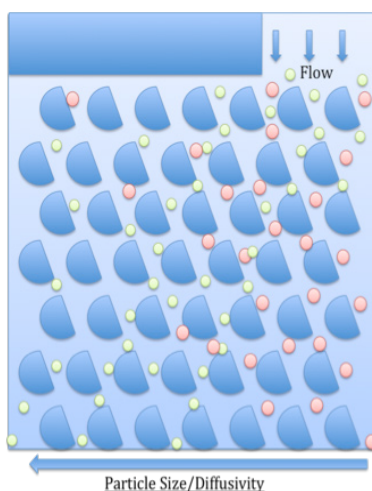


Fig. 1 — Brownian ratchets are asymmetric shapes that help to facilitate biased diffusion

This report summarizes the results of the studies conducted, including two generations of the ratchet devices and four different chemical functionalities. The devices were used to alter concentration profiles for polystyrene nanoparticles in aqueous solutions. Key parameters such as ratchet feature size, flow rate, and particle concentration were evaluated. This study demonstrated that nondeterministic separation has potential for application to continuous separation of nanoparticle materials. In addition, it demonstrated that chemical surface functionalities can be used to significantly alter the performance of the devices.

APPROACH

Reagents

Hydrogen peroxide (30%), sulfuric acid, sodium phosphate dibasic, and sodium phosphate monobasic were obtained from Sigma-Aldrich (St. Louis, MO). Carboxyethylsilanetriol (CES), 3-aminopropyltriethoxysilane (APS), nonafluorohexyltriethoxysilane (NFS), and phenyltrimethoxysilane (PTS) were obtained from Gelest (Morrisville, PA; Fig. 2). Carboxyl orange fluorescent polystyrene nanospheres were manufactured by Phosphorex (Hopkinton, MA). The nanoparticles had a diameter of 40 nanometers (nm) with an excitation wavelength of 460 nm and an emission wavelength of 500 nm. All chemicals were used as received. Water was deionized to 18.2 M Ω using a Mill-Q water purification system. Buffer solutions at the three pH values described (6.5, 7.5, and 9.5) were prepared through mixing of 0.5 M sodium phosphate monobasic and dibasic solutions. These stock solutions were diluted to obtain 50 mM final concentrations for the experimental samples.

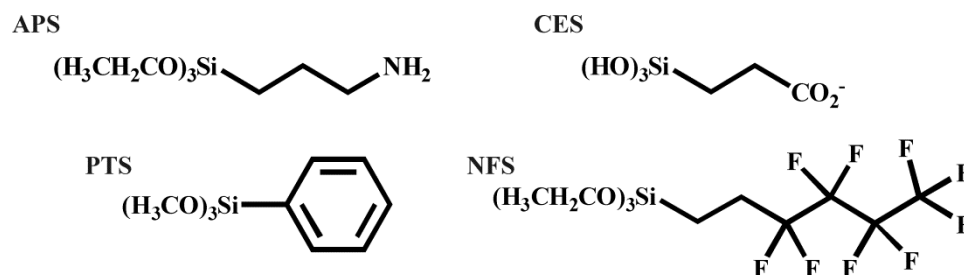


Fig. 2 — Structures of siloxane compounds used for slide and wafer functionalization

Fluorescence

The as-received nanoparticle solution was 1% solids. This solution was diluted 7 μL into 50 mL deionized water to produce a stock solution of 1.11×10^{16} particles per liter (p/L). This stock and two dilutions of this stock (1:500, 2.2×10^{13} p/L and 1:50, 2.2×10^{14} p/L) were utilized in experiments. A calibration curve relating the fluorescence of the solutions to the concentration of the nanoparticles was collected for each experiment (Fig. 3). This curve was prepared in the microtiter plate used for the experimental samples and was measured during analysis of the experimental results. The calibration curve consisted of six points prepared by serial dilution (2 \times each step) of the solution prepared for the experiment. A linear fit of the resulting data utilized as fluorescence intensity versus nanoparticle concentration was generated for each of these curves (slope = 1×10^{-10} ; y-intercept = 3965). The variation between experiments was approximately 10%; variations within a single experiment were less than 3%. Fluorescence measurements were completed using a Tecan XSafire microtiter plate reader with appropriate excitation and emission wavelengths (10 nm bandwidth). The gain was set to 224, integration time was 20 μs , and the z-position was 19488 μm .

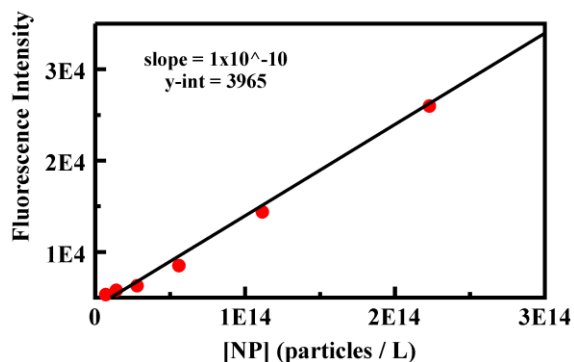


Fig. 3 — Representative calibration curve for the fluorescent nanospheres utilized in these studies. Diameter 40 nm, excitation wavelength 460 nm, emission wavelength 500 nm.

Asymmetric Ratchet Devices

Two generations of ratchet devices were fabricated for the work described in this report. For the first generation of devices, the fabrication process began by creating masks for pattern transfer. Two families of masks were produced: fields of ratchets and blank fields (channels). Fabrication procedures were the same for both masks. Masks were drawn in Inventor (Autodesk, San Rafael, CA) and printed on transparencies (resolution better than 5080 dpi) using a commercial vendor (PageWorks, Cambridge, MA). These transparency masks were taped to a blank 5 in. by 5 in. plate and secured directly into a commercial mask holder (ABM Mask Aligner, Scotts Valley, CA) for pattern transfer. Devices were fabricated on glass microscope slides. Borosilicate, soda lime, and quartz slides were evaluated, and etch rates, surface roughness, and uniformity were considered. Etch rates on quartz slides were extremely slow while the borosilicate slides produced features with significant roughness. The best results were obtained with soda lime glass substrates (Ted Pella Inc., Redding, CA). Evaluations also showed that the desirable etch depth ($\sim 5 \mu\text{m}$) could not be obtained using a photoresist mask. A metal mask was instead transferred to the glass substrates using a lift-off process (Fig. 4) [16].

Soda lime glass microscope slides (1 in. \times 3 in.) were extensively cleaned for at least 3 hours in piranha solution (30% hydrogen peroxide and 70% sulfuric acid) followed by copious rinsing with deionized water. Negative photoresist (product NR-7 P1000, Futurrex Inc., Franklin, NJ) was spun onto the substrates using the manufacturer's recommended protocol. The photoresist was patterned on a mask aligner with 365 nm light and developed in RD6 solution (Futurrex, Inc.). A thin layer of gold (100 nm) with an adhesion layer of chromium (30 nm) was deposited on the slides using an electron-beam evaporator (Temescal, model FC-2000, Livermore, CA). Chromium was chosen as an adhesion layer because it was found to be more resistant than titanium to the glass etchants. The glass slides were placed in an acetone bath to dissolve the photoresist and transfer the ratchet pattern onto the slides by a lift-off process. Glass slides with metal feature masks were etched in buffered oxide etch (BOE) solution with constant stirring (BOE:HCl:H₂O 1.5:1:6 by vol.). These conditions resulted in etch rates of 1.25 to 1.5 $\mu\text{m}/\text{min}$. Slower etch rates and the presence of hydrochloric acid were found to reduce surface roughness following the etch process. Slides were thoroughly cleaned in deionized water and sequentially placed in warm (40 °C) aqua regia solution (HCl:HNO₃ 3:1) and chrome etch (CR-9, Cynatek Corp., Fremont, CA) to remove the Au and Cr layers, respectively. Finally, slides were cleaned in piranha solution, rinsed, and dried (Fig. 5).

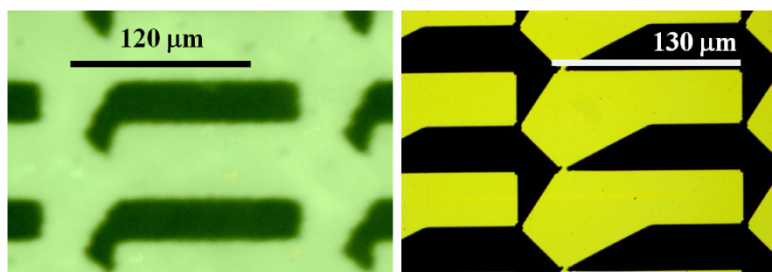


Fig. 4 — In the original masks (left), the isotropic oxide etch caused undercut of the design, resulting in a loss of the head shape for the asymmetric features. The undercut also left the features fragile. The oversized mask (right) compensates for the undercut. Adjacent ratchets are joined in the mask. The features resulting from isotropic oxide etching of this mask are roughly trapezoidal with the base larger than the top surface.

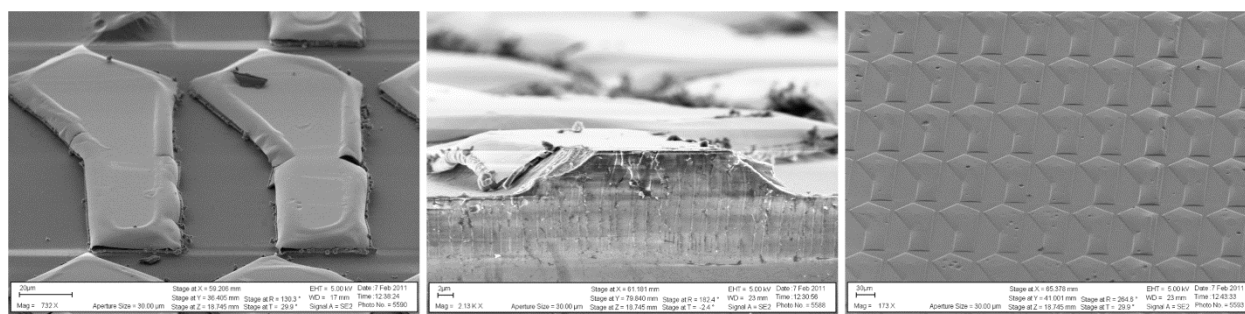


Fig. 5 — An Au/Cr mask was used to etch the soda lime slides with hydrogen fluoride solutions. The isotropic etch process undercuts the mask which is still in place in this image (left). In the cross-sectional view of a single ratchet (center), the trapezoidal shape can be seen prior to stripping of the Au/Cr mask. After stripping of the mask (right), the individual ratchets in the field are separated from one another.

For the second generation of devices, patterns were drawn in L-Edit software (Tanner EDA, Monrovia, CA). These patterns were converted to GDSII format, used to expose glass photomask blanks on a Heidelberg DWL-66 Laser Pattern Generator (Heidelberg Instruments, Heidelberg, Germany), developed with AZ developers, and etched with CR-9 chrome etchant using standard procedures. Second generation ratchet devices were fabricated on 4 in. silicon wafers. Similarly to the glass slides, they were first cleaned, dried, and patterned with NR-7 photoresist. In this case, however, material was removed from the silicon wafers using the Bosch DRIE process in a plasma assisted deep reactive ion etching station (Oxford Instruments, Tubney Wood, Abingdon, UK). The chosen conditions allowed etch rates of roughly 1 to 1.25 $\mu\text{m}/\text{step}$. After etching, the wafers were stripped of excess photoresist and cleaned in an oxygen plasma.

During process development, ratchet devices were characterized by both light and electron microscopy to verify the integrity of the ratchet shape after etching. Fabrication conditions were adjusted until the desired geometry was realized in the substrates. For the first generation glass devices, the mask features were made larger (1:1.5) to compensate for lateral etch due to the isotropic nature of the wet etch process, and features with curved side walls resulted. The Bosch DRIE process is inherently anisotropic

and produced features with near-vertical sidewalls. The etch depths for each slide/wafer were measured with a surface profilometer (KLA-Tencor, model Alpha-Step 500, Milpitas, CA). Etch depths for glass devices were found to range between 4 and 6 μm and, in some cases, exhibited considerable variability field. The DRIE process produced depths of 5 to 10 μm with high uniformity across a single wafer as well as high reproducibility across multiple wafers. The glass devices proved desirable for transparency; however, the lack of uniformity of the features was a concern.

Custom holders for the devices of both generations were fabricated in Plexiglas-G and sealed with O-rings (Fig. 6). This particular plastic was chosen because it is transparent, allowing the experiment to be observed. Dispensing syringe tips (Nordson EFD, Westlake, OH) were inserted into the holders to facilitate connections to silicone tubing.

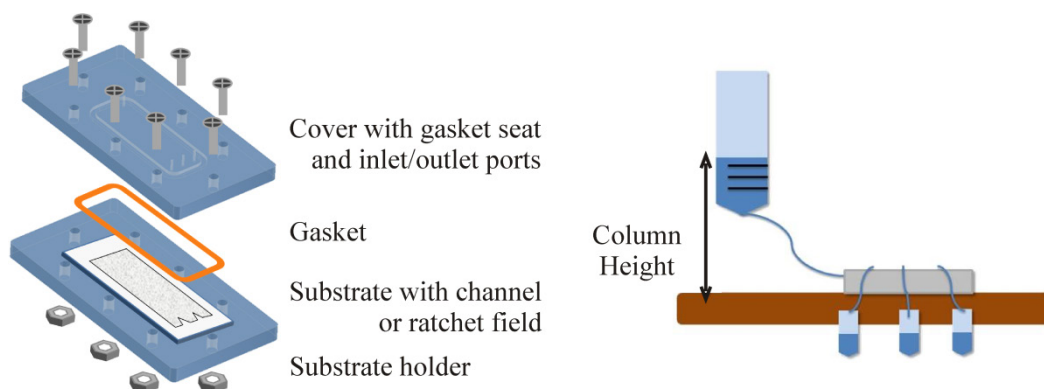


Fig. 6 — Left: The assembly for the generation 1 glass devices. The assembly for generation 2 silicon devices is identical except for dimensions. Right: The experimental setup including the water column and the collection vessels.

Surface Functionalization

Etched devices were cleaned prior to use in experiments by soaking in piranha solution for 30 min. Following the piranha bath, devices were repeatedly rinsed in deionized water and dried at 110 $^{\circ}\text{C}$. Functionalization of wafers was accomplished by immersing the wafer in a solution of 20 mM silane precursor (CES, APS, PTS, or NFS) in toluene for 45 min. The wafers were then dipped sequentially in toluene baths (3) to remove excess solution and dried at 110 $^{\circ}\text{C}$ overnight. Both ratchet-bearing and channel-only wafers were functionalized using each of the precursors. Functionalization of slides was accomplished similarly; however, concentrations of 50 and 150 mM APS, PTS, and NFS were utilized.

Experimental Setup

For both device generations, the experimental setup utilized a 60 mL syringe as a sample reservoir. The flow rate was controlled through adjusting the distance between the top of the fluid column and the device entry point (Fig. 6). This was accomplished by altering the fill volume of the syringe or through changing the height of the syringe above the device. Tubing (Tygon, formula R-3603, ID = 0.0173 in., OD = 0.0893 in., Cole-Parmer, Vernon Hills, IL) connected the syringe to the inlet port and the three outlet ports to the collection vials (typically Eppendorf tubes). All solutions were de-gassed in a vacuum oven prior to use; air in the devices was found to result in inconsistent flow rates. For the first generation glass devices, 1 mL of the solution being used was allowed to pass through the device so that the system

could come to equilibrium before samples were collected. For each trial, the solution flow time was measured and the individual collection vessels were weighed before and after filling so that flow rates could be monitored. The second generation wafer devices were used similarly with one exception. The equilibrium time was extended to 1 h prior to sample collection. For the generation 1 glass devices, flow rates between 0.22 and 0.24 mL/min were utilized in all cases. Flow rates for the generation 2 devices are specified in the figures.

EXPERIMENTS

Generation 1 Glass Devices

Initial analysis compared the concentrations at the three exit ports from the device to the initial concentration of the nanoparticle solution. It is important to note that the inlet port on the device must be oriented on the short side of the asymmetric features. Altering this orientation strongly impacts the performance of the device. With the device in an improper orientation, i.e., with the inlet port on the long side of the features, a random distribution of concentrations is obtained. When the device was evaluated in the proper orientation, a slight increase in concentration (1.5%) was noted for the outlet port furthest from the inlet port while the outlet port closest to the inlet port had a slightly reduced concentration (Fig. 7).

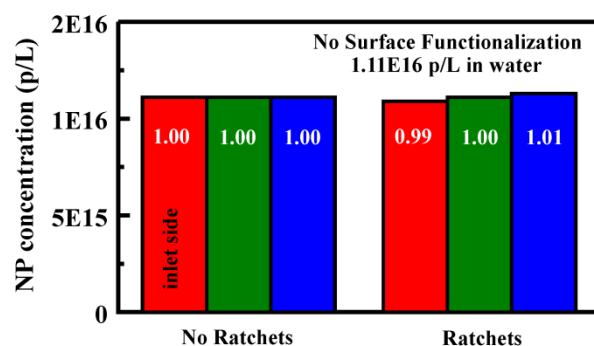


Fig. 7 — Nanoparticle concentrations at the three exit ports for generation 1 glass devices with a channel only and with a ratchet field. Initial particle concentration was 1.11×10^{16} p/L in water. Data presented is the average of three experiments.

The generation 1 glass devices were functionalized with APS, PTS, and FNS in order to evaluate the potential of chemical surface functionality for enhancing separation efficiencies. These changes in chemical functionality produced very little change in the particle distributions across the three exit ports (Fig. 8). In fact, although the data set did serve to confirm the enhanced concentration noted at the furthest outlet port in Fig. 7, no definitive improvement due to surface functionalization could be determined. Because both the nanoparticles and the APS functionalized surfaces bear charged groups, it was thought that altering the pH of the nanoparticle solutions might serve to enhance the biased diffusion of particles. Solution pHs of 4.5, 7.0, and 8.5 were considered. At low pH (4.5), the nanoparticles were observed to precipitate from solution. As a result, this solution was discarded. Results for solutions at pH 7.0 and 8.5 are presented in Fig. 9. Altering the pH of the samples produced little change in the concentration profiles. The slight changes in concentration noted for these devices, regardless of functionalization or charge, were well below what was expected.

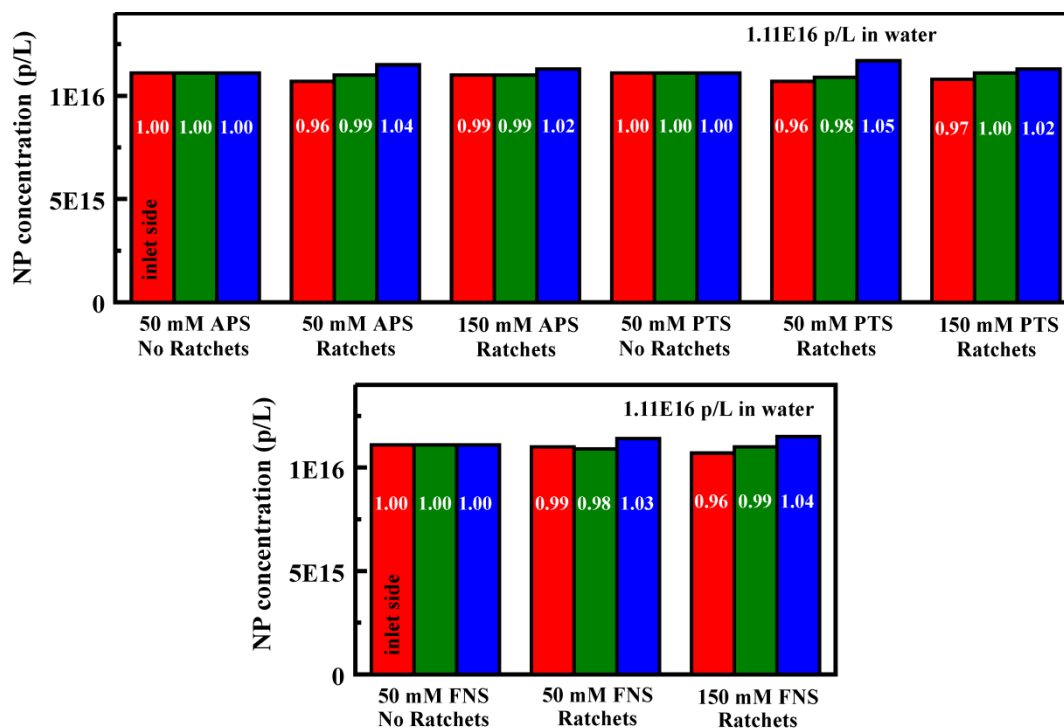


Fig. 8 — Nanoparticle concentrations at the three exit ports for generation 1 glass devices with a channel only and with a ratchet field bearing varied surface functionalities. Initial particle concentration was 1.11×10^{16} p/L in water. Data presented is the average of three experiments.

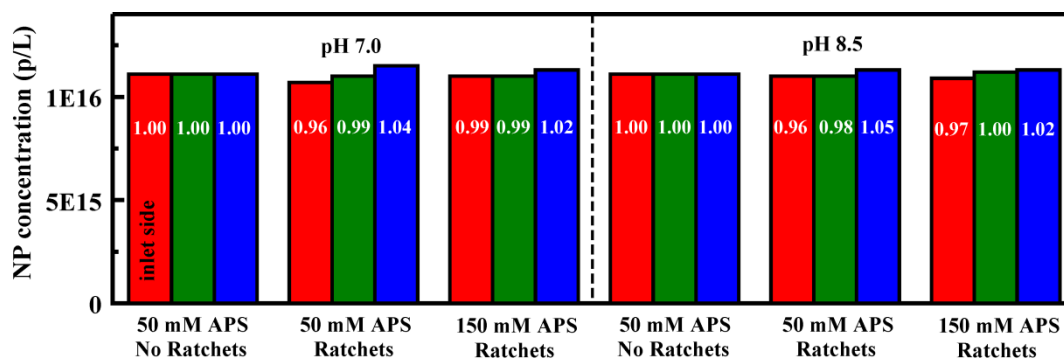


Fig. 9 — Nanoparticle concentrations at the three exit ports for generation 1 glass devices with a channel only and with a ratchet field for solutions at varied pH. Initial particle concentration was 1.11×10^{16} p/L in water. Data presented is the average of three experiments.

Generation 2 Silicon Devices

A number of factors were considered with a view toward improvement of the results achieved with the generation 1 glass devices. First, the generation 2 silicon devices offer a ratchet field that is 7.48 cm long as compared to the 4.45 cm fields of the generation 1 devices (field widths were 1.4 cm). Second, the experiments with the generation 2 devices utilized an equilibration time of 1 h before collection of data.

This provided the potential to completely flush previously used solutions as well as to establish behaviors that may not be observed during the introduction of new solutions. Finally, functionalization of the wafers using carboxyl groups was evaluated, in addition to the amine, phenyl, and fluorine considered above. These various functional groups were expected to produce unique interactions with the carboxyl groups on the surface of the nanoparticles. It was also expected that changing the protonation state of the carboxyl groups (pH) and the surfaces would produce changes in the interactions with the device surfaces.

Surface Functionalization

Initial studies using the ratchet devices with no surface functionalization and nanoparticle solutions in deionized water saw differences in concentration across the exit ports that were greater than those observed with the generation 1 devices. Enhancements on the order of 6 to 12% were noted (Fig. 10). While these differences were larger than those observed for the generation 1 glass devices, further enhancement would be desirable.

Similar experiments were completed for wafers functionalized with APS, CES, PTS, and NFS. The results (Fig. 10) were similar to those obtained for the unfunctionalized wafers. APS functionalized wafers showed a 28% greater concentration of nanoparticles at the outlet port furthest from the inlet side of the device than that obtained for the port on the inlet side. CES functionalized wafers showed a 9% greater concentration of nanoparticles at the furthest exit port.

Surface Charge

Initial experiments utilizing unfunctionalized wafers found that changing the pH of the nanoparticle solution to 5.0 produced striking changes in the particle distribution across the exit ports. It was found that pH values below 6.0, in fact, cause precipitation of the nanoparticles from the aqueous solution and lead to these unusual particle distributions. For this reason, pH values of 6.5, 7.5, and 9.5 were utilized. Though pH 6.5 does not provide fully protonated nanoparticles, it should be sufficient to determine if the change in protonation has an impact. In addition, for the functionalized surfaces (amine and carboxyl groups), the protonation state of these groups is expected to change across this pH range as well. Changing the pH of the nanoparticle solutions did not significantly impact the concentration distributions for the unfunctionalized wafers. The NFS and PTS functionalized wafers were not evaluated with the pH controlled solutions. As shown in Fig. 11, Fig. 12, and Fig. 13, however, solution pH did have an impact on concentration profiles across the CES and APS wafers.

The APS device and the nanoparticles bear opposite charges. As pH is decreased, the nanoparticles become more neutral while the surface becomes more positively charged. Conversely, as the pH is increased, the surface becomes more neutral while the particles become more negatively charged. As shown in Fig. 12, the pH 7.5 nanoparticle solution resulted in the greatest difference in concentration across the exit ports. This is likely the pH at which both the surface and the particles are significantly charged. For pH 6.5 (Fig. 11), the difference in concentration across the outlet ports was somewhat smaller, and for pH 9.5 (Fig. 13), concentrations at the three ports were similar.

The CES device and the nanoparticles both bear carboxylate groups and, therefore, similar charge. The difference in the environments of those groups causes the pKa of those charged groups to vary somewhat. This is reflected by the changing concentration profiles as the pH of the solution is shifted. As shown in Fig. 11, the pH 6.5 nanoparticle solution resulted in the greatest difference in concentration across the exit ports. The outlet port furthest from the inlet side of the device had an 80% greater concentration of nanoparticles than that obtained for the port on the inlet side. For pH 7.5 (Fig. 12), this difference was somewhat smaller, and for pH 9.5 (Fig. 13), the behavior was similar to that observed for the unfunctionalized surfaces.

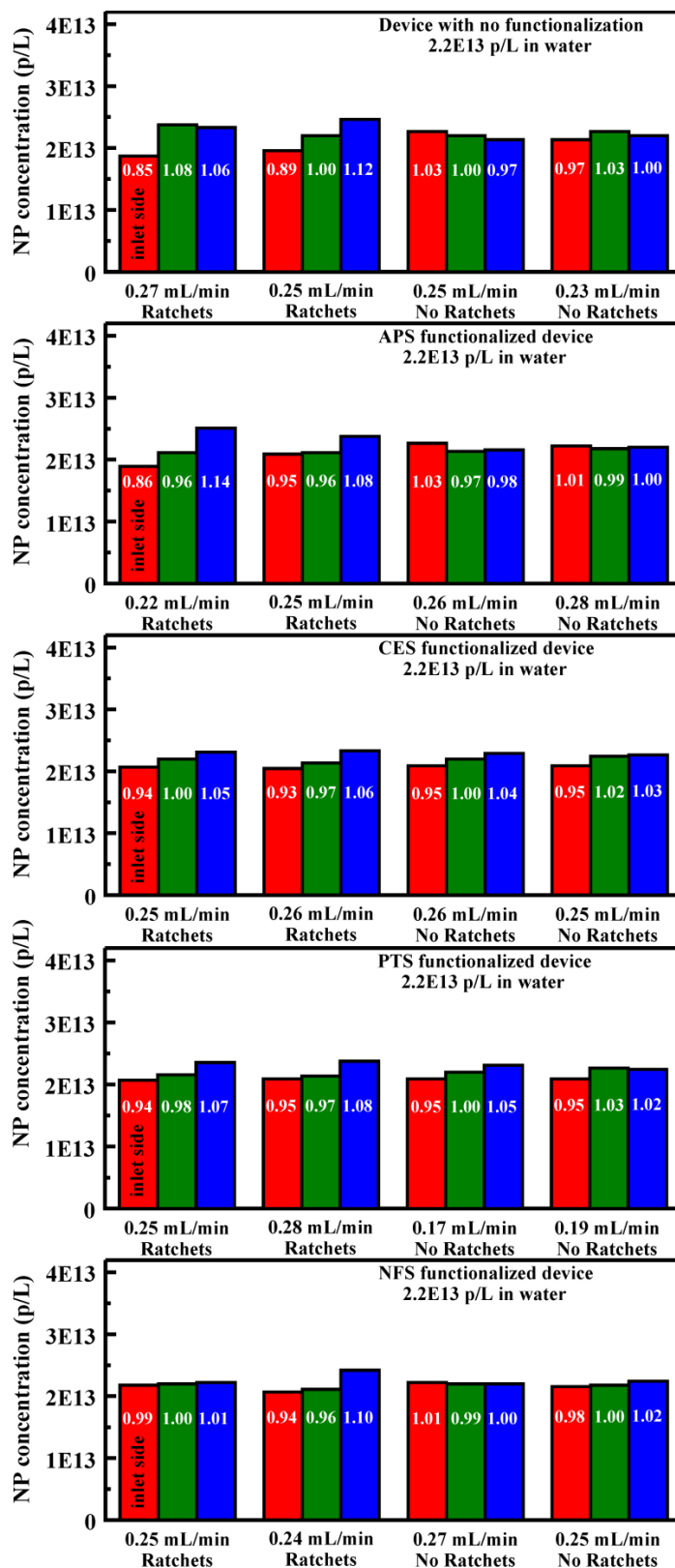


Fig. 10 — Concentrations of nanoparticles for each of the three exit ports are presented. Shown here are nanoparticles in water on functionalized and unfunctionalized generation 2 devices. Data represents the average of a minimum of three experiments.

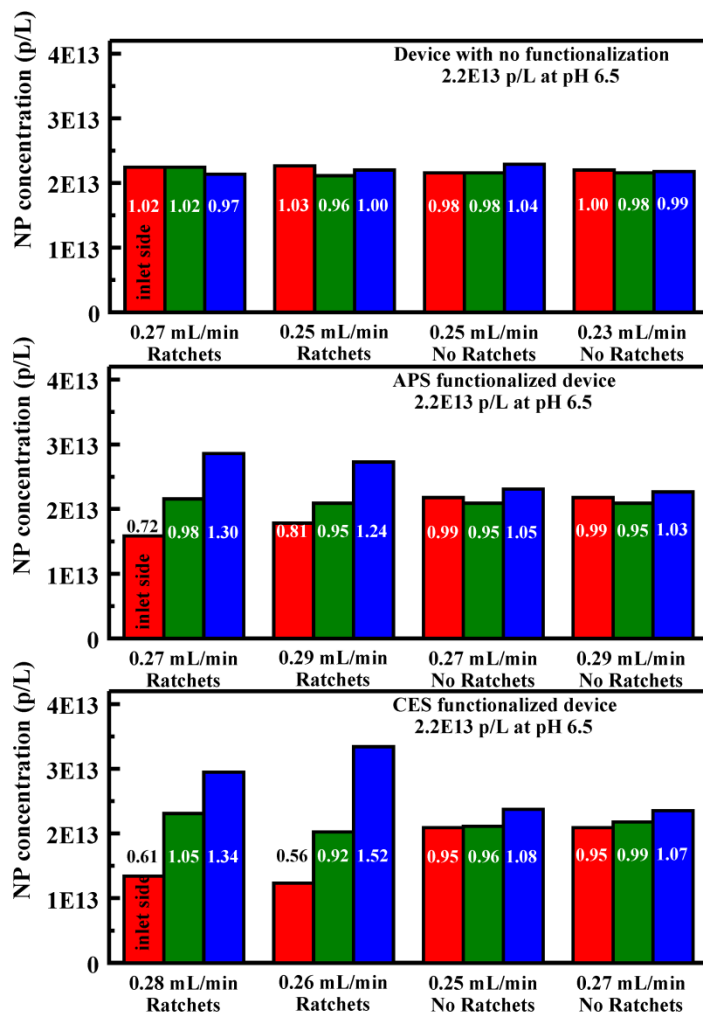


Fig. 11 — Concentrations of nanoparticles for each of the three exit ports are presented. Shown here are results for nanoparticle solutions at pH 6.5 on generation 2 devices bearing different surface functionalities. Data represents the average of a minimum of three experiments.

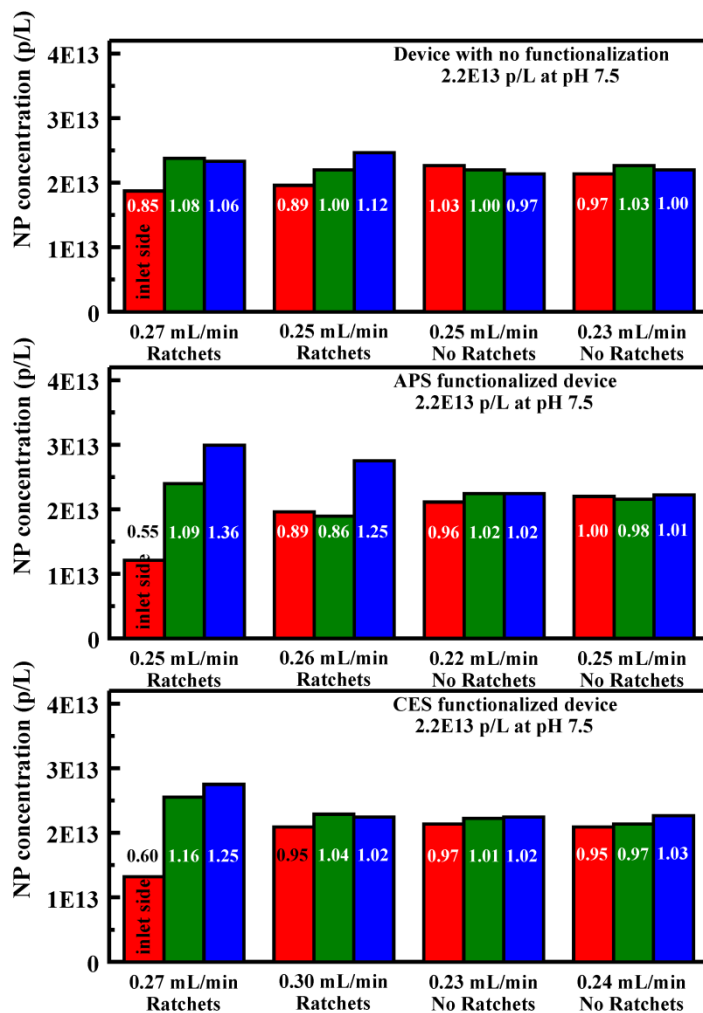


Fig. 12 — Concentrations of nanoparticles for each of the three exit ports are presented. Shown here are results for nanoparticle solutions at pH 7.5 on generation 2 devices bearing different surface functionalities. Data represents the average of a minimum of three experiments.

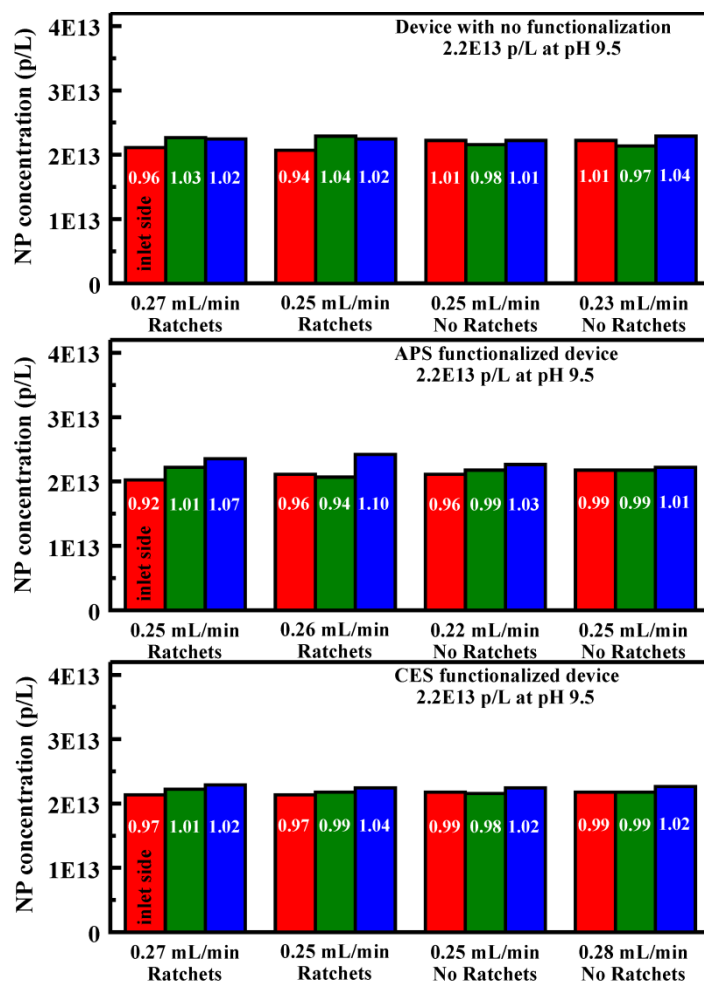


Fig. 13 — Concentrations of nanoparticles for each of the three exit ports are presented. Shown here are results for nanoparticle solutions at pH 9.5 on generation 2 devices bearing different surface functionalities. Data represents the average of a minimum of three experiments.

Other Considerations

In addition to surface functionalization and protonation state, two other considerations were of interest here: flow rate and nanoparticle concentration. First, the flow rate in the device was an acknowledged consideration based on the results noted for the generation 1 glass devices. Separations were strongly dependent on achieving slow, controlled flow. Maintaining consistent flow through the device required a minimum driving force with an associated minimal flow rate. The data presented in Fig. 10, Fig. 11, Fig. 12, and Fig. 13 provide two flow rates for each condition considered. While flow rates below 0.20 mL/min tended to result in cessation of flow from one or more of the exit ports in the ratchet devices, flow rates of as little as 0.17 mL/min were sufficient in the channel-only devices. This is likely a result of the increased back pressure in the ratchet-bearing devices. If the results in Fig. 11 are taken as an example, the impact of increasing flow rate becomes apparent. For the APS functionalized device, the concentration at the farthest exit port is lower for experiments at 0.29 mL/min as compared to those at 0.27 mL/min. Similarly, for the CES functionalized device, the concentration at the furthest exit port is lower for experiments at 0.28 mL/min than for those at 0.26 mL/min.

The second of these considerations arose from a mistake in the laboratory. Fluorescence data at levels well below those adhering to the standard calibration curve were obtained with associated improvements in the concentration enhancements observed. A mistake in the preparation of the nanoparticle solution was suspected. As a result, a series of experiments were compared using 2.3×10^{14} and 2.3×10^{13} p/L concentrations. It was found that at lower concentrations of nanoparticles, the shift in the concentration profile was significantly enhanced (Fig. 14, Fig. 15, Fig. 16, and Fig. 17). This may be related to the frequency of collisions between particles in solution and the impact of those collisions on the efficiency of the asymmetric shapes within the ratchet field. If the results from Fig. 11 are compared to those presented in Fig. 15 for the same devices at similar flow rates and identical pH, we see that for the APS functionalized device, the concentration enhancement at the exit port drops from 1.30 to 1.04 (0.27 mL/min) when nanoparticle concentration is increased by an order of magnitude. A similar drop in enhancement (1.52 to 1.09 at 0.26 mL/min) can be seen for the CES functionalized device.

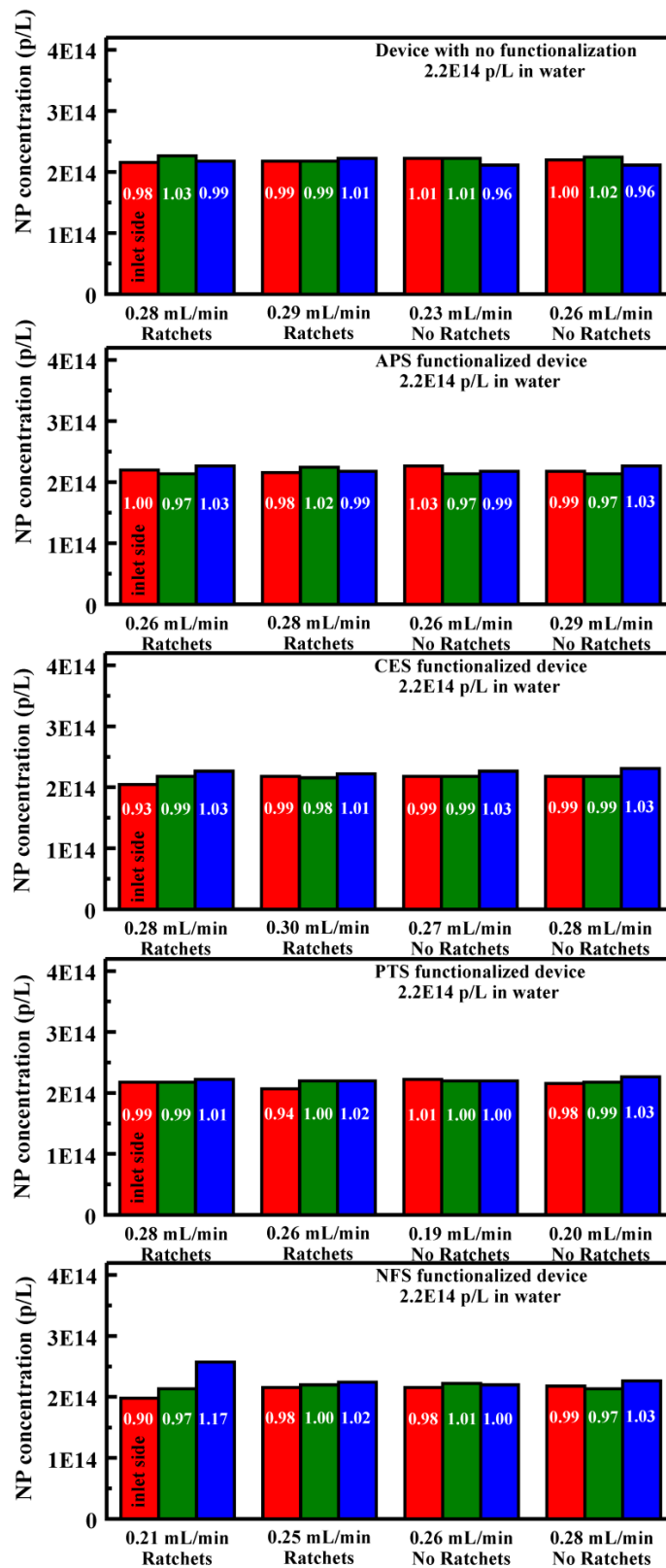


Fig. 14 — Concentrations of nanoparticles for each of the three exit ports are presented. Shown here are results for nanoparticle solutions at 2.2×10^{14} p/L. Compare to results in Fig. 10. Data represents the average of a minimum of three experiments.

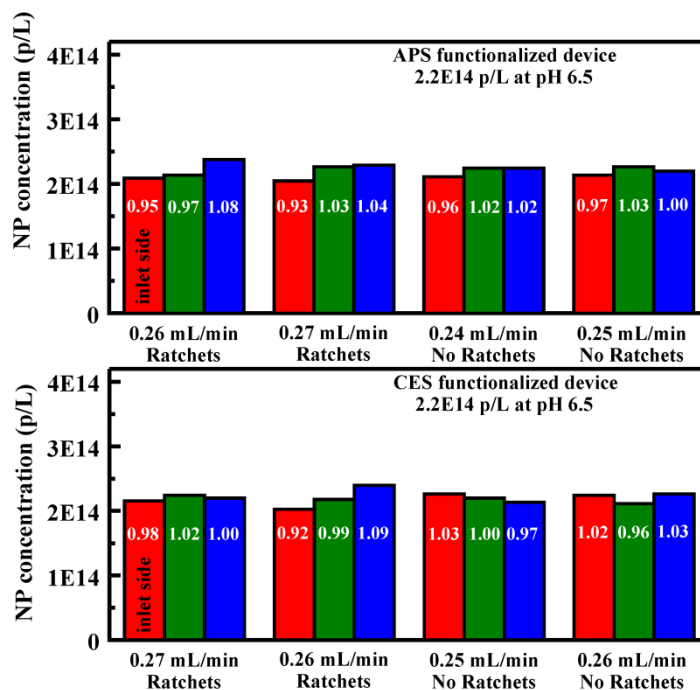


Fig. 15 — Concentrations of nanoparticles for each of the three exit ports are presented. Shown here are results for nanoparticle solutions at 2.2×10^{14} p/L. Compare to results in Fig. 11. Data represents the average of a minimum of three experiments.

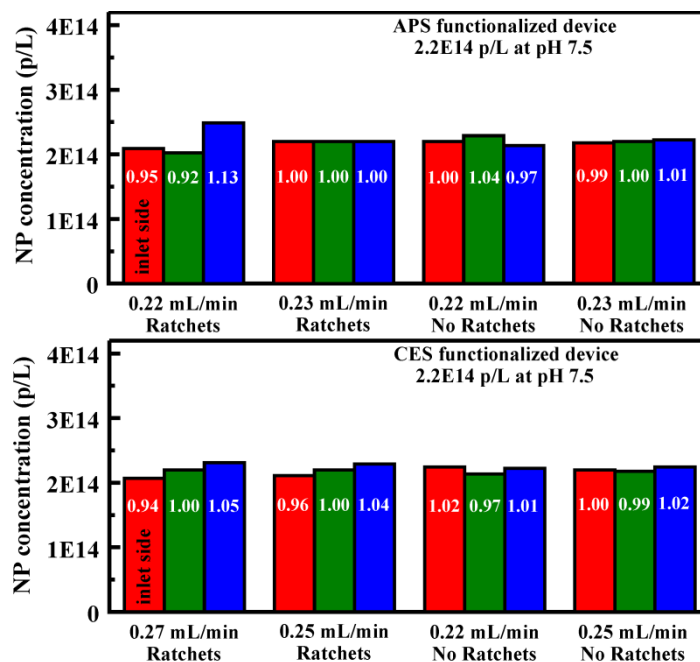


Fig. 16 — Concentrations of nanoparticles for each of the three exit ports are presented. Shown here are results for nanoparticle solutions at 2.2×10^{14} p/L. Compare to results in Fig. 12. Data represents the average of a minimum of three experiments.

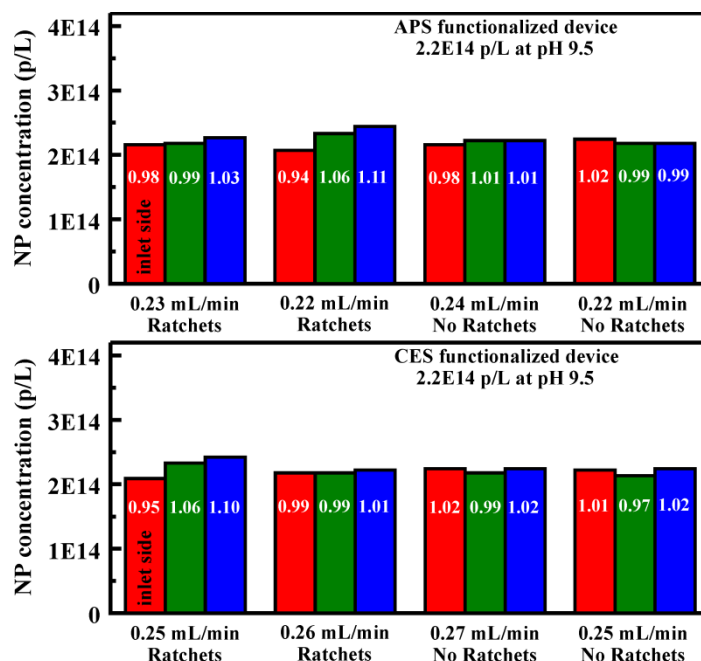


Fig. 17 — Concentrations of nanoparticles for each of the three exit ports are presented. Shown here are results for nanoparticle solutions at 2.2×10^{14} p/L. Compare to results in Fig. 13. Data represents the average of a minimum of three experiments.

CONCLUSIONS

This study demonstrated that it is possible to bias the diffusion of nanoparticles using Brownian motion to achieve a nondeterministic separation technique. The results presented here further demonstrate that combining the asymmetric mechanical component with chemical functionality and control of protonation states can provide greatly enhanced performance from the device. The most significant separation was achieved using a carboxyl functionalized device to separate carboxyl functionalized nanoparticles in a solution pH of 6.5. This set of experimental conditions produced a difference of 2.11×10^{13} p/L between the inlet and outlet side ports. This resulted from a 44% reduction in concentration at the inlet side port and a 52% increase in concentration at the outlet side port. It was also shown that flow rates and particle concentrations must be carefully considered.

It is likely that experiments in which nanoparticles traverse a longer field of ratchets will result in even more significant concentration enhancements. Future experiments could also potentially use multiple functionalizations simultaneously to observe separation in different directions. Here, a single type of nanoparticle was in each experiment. If multiple particles bearing different functional groups were utilized, separation potential could be evaluated. Experiments using particles of varying size would also be of interest. Future experiments could also use different functionalized wafers to observe more patterns; for example, phenyl and fluorinated groups produced little of interest to these studies. Other groups, for example a branched amine bearing compound, may produce greater enhancements.

The use of Brownian ratchets to separate particles in solution is novel; previous descriptions and studies have focused on particles in air. This type of system could provide the potential to separate, concentrate, or recover nanoparticles from solution following a single use or even following synthesis or modification. With more research, Brownian ratchets could prove to be more effective than some existing technologies due to the potential for continuous separation as opposed to the batch type separation that is

more commonly used in current approaches. Novel technologies using Brownian ratchets could provide chromatographic solutions such as target enrichment, but at a lower cost and at higher overall yield. Batch separations and analyses could also be conducted to yield macro-level filtration.

ACKNOWLEDGMENTS

Carrie Sun and Connie Scoggins (Thomas Jefferson High School for Science and Technology, Alexandria, VA) participated in this effort through the U.S. Navy Science and Engineering Apprenticeship Program (SEAP). Jason E. Bongard (NOVA Research, Inc.) participated in development of the initial concepts that resulted in the research described here. Mansoor Nasir (formerly NRL, currently Lawrence Technological University, Southfield, MI) developed the generation 1 devices. Martin H. Moore (NRL) provided technical support for device functionalization. This research was sponsored by the U.S. Office of Naval Research through Naval Research Laboratory base funds (69-9899).

REFERENCES

1. R. D. Astumian and I. Derenyi, 1998, "Fluctuation driven transport and models of molecular motors and pumps," *European Biophysics Journal With Biophysics Letters* 27(5), 474–489. doi: 10.1007/s002490050158.
2. J. P. Beech and J. O. Tegenfeldt, 2008, "Tuneable separation in elastomeric microfluidics devices," *Lab on a Chip* 8(5), 657–659. doi: 10.1039/b719449h.
3. P. S. Burada, G. Schmid, D. Reguera, J. M. Rubi, and P. Hanggi, 2007, "Biased diffusion in confined media: Test of the Fick-Jacobs approximation and validity criteria," *Physical Review E* 75(5). doi: 10.1103/PhysRevE.75.051111.
4. M. Cabodi, Y. F. Chen, S. W. P. Turner, H. G. Craighead, and R. H. Austin, 2002, "Continuous separation of biomolecules by the laterally asymmetric diffusion array with out-of-plane sample injection," *Electrophoresis* 23(20), 3496–3503. doi: 10.1002/1522-2683(200210)23:20<3496::aid-elps3496>3.0.co;2-9.
5. J. A. Davis, D. W. Inglis, K. J. Morton, D. A. Lawrence, L. R. Huang, S. Y. Chou, J. C. Sturm, and R. H. Austin, 2006, "Deterministic hydrodynamics: Taking blood apart," *Proceedings of the National Academy of Sciences of the United States of America* 103(40), 14779–14784. doi: 10.1073/pnas.0605967103.
6. I. Derenyi and R. D. Astumian, 1998, "ac separation of particles by biased Brownian motion in a two-dimensional sieve," *Physical Review E* 58(6), 7781–7784. doi: 10.1103/PhysRevE.58.7781.
7. F. Family, H. A. Larrondo, D. G. Zarlenga, and C. M. Arizmendi, 2005, "Chaotic dynamics and control of deterministic ratchets," *Journal of Physics: Condensed Matter* 17(47), S3719–S3739. doi: 10.1088/0953-8984/17/47/006.
8. L. R. Huang, E. C. Cox, R. H. Austin, and J. C. Sturm, 2003, "Tilted Brownian ratchet for DNA analysis," *Analytical Chemistry* 75(24), 6963–6967. doi: 10.1021/ac0348524.
9. L. R. Huang, E. C. Cox, R. H. Austin, and J. C. Sturm, 2004, "Continuous particle separation through deterministic lateral displacement," *Science* 304(5673), 987–990. doi: 10.1126/science.1094567.

10. M. Kersaudy-Kerhoas, R. Dhariwal, and M. P. Y. Desmulliez, 2008, "Recent advances in microparticle continuous separation," *IET Nanobiotechnology* 2(1), 1–13. doi: 10.1049/iet-nbt:20070025.
11. S. Matthias and F. Muller, 2003, "Asymmetric pores in a silicon membrane acting as massively parallel brownian ratchets," *Nature* 424(6944), 53–57. doi: 10.1038/nature01736.
12. N. Pamme, 2007, "Continuous flow separations in microfluidic devices," *Lab on a Chip* 7(12), 1644–1659. doi: 10.1039/b712784g.
13. S. Savell'ev, V. Misko, F. Marchesoni, and F. Nori, 2005, "Separating particles according to their physical properties: Transverse drift of underdamped and overdamped interacting particles diffusing through two-dimensional ratchets," *Physical Review B* 71(21). doi: 10.1103/PhysRevB.71.214303.
14. S. Sengupta, R. Guantes, S. Miret-Artes, and P. Hanggi, 2004, "Controlling directed transport in two-dimensional periodic structures under crossed electric fields," *Physica A: Statistical Mechanics and Its Applications* 338(3–4), 406–416. doi: 10.1016/j.physa.2004.02.063.
15. J. O. Tegenfeldt, C. Prinz, H. Cao, R. L. Huang, R. H. Austin, S. Y. Chou, E. C. Cox, and J. C. Sturm, 2004, "Micro- and nanofluidics for DNA analysis," *Analytical and Bioanalytical Chemistry* 378(7), 1678–1692. doi: 10.1007/s00216-004-2526-0.
16. P. C. H. Li, *Microfluidic Lab-on-a-Chip for Chemical and Biological Analysis and Discovery* (CRC Press, Boca Raton, FL, 2006).